Square-Root Algorithm for Evaluating Mismodeled Process Noise

C. L. THORNTON* AND S. G. FINLEY†
Jet Propulsion Laboratory, Pasadena, Calif.

Unmodeled random accelerations acting on spacecraft place severe limitations on the application of classical least squares filters to interplanetary navigation. Various modified Kalman filters have been developed which attempt to model the random process affecting the spacecraft state. As the application of sequential filters has grown, the need has arisen to evaluate the sensitivity of these filters to mismodeling of the random process. In this paper a numerically reliable square-root algorithm is presented for calculating the covariances of estimates from a sequential filter which incorrectly models process noise. Mismodeling is restricted to the correlation time and standard deviation of a random process represented as a first-order Gauss-Markov sequence. Using a computer program which employs this algorithm, a sensitivity analysis was performed for several types of Earth-based tracking data from an interplanetary spacecraft.

Nomenclature

p_i = first-order Gauss-Markov sequence of random accelerations affecting the spacecraft
τ = correlation time of the sequence p_i
w_i = white noise which drives p_i
Λ_p = covariance of p_i assumed by the filter
$\bar{\Lambda}_p$ = true covariance of p_i
Λ_w = covariance of w_i assumed by the filter
$\bar{\Lambda}_w$ = true covariance of w_i
y_i = sequence of parameter vectors
z_i = sequence of observation vectors
n_i = measurement errors of z_i
A_i = partial derivatives of z_i with respect of y_i
$\tilde{z}_i$ = a priori data, a linear combination of $z_j, j < i$
$\tilde{n}_i$ = error in $\tilde{z}_i$
$\tilde{n}_a(i)$ = actual error in $\tilde{z}_i$
$\tilde{y}_i$ = a priori estimate of y_i, before z_i is included
$\tilde{\Lambda}_i$ = covariance of $\tilde{y}_i$
v = norm of residual vector
$\hat{y}_i$ = linear minimum variance estimate of y_i, given $z_j, j \leqq i$.
Λ_i = covariance of $\hat{y}_i$, computed by filter
$\bar{\Lambda}_i$ = true or actual covariance of $\hat{y}_i$, given $\bar{\Lambda}_w$ and $\bar{\phi}_{i+1,i}$
$\phi_{i+1,i}$ = state transition matrix assumed by filter
$\bar{\phi}_{i+1,i}$ = true state transition matrix
R_i = square-root of the information matrix, called the information array
$\bar{R}_i$ = actual information array after including the data, z_i
z_i' = linear combination of z_i and $\tilde{z}_i$
n_i' = error in z_i' assumed by the filter
$n_a(i)$ = actual error in z_i'
$R_{yw}(i)$ = square-root of the covariance of a linear combination of n_i' and w_i, used to compute $\bar{\Lambda}_{i+1}^{-1/2}$
ξ_i = linear combination of $n_a(i)$ and p_i; a vector of the actual data errors, needed to compute $\bar{\Lambda}_i$
Λ_ξ = covariance of ξ_i
QVLBI = refers to data which include nearly simultaneous range and doppler measurements
Differenced-*QVLBI* = refers to data containing explicitly differenced simultaneous doppler and/or range measurements
CLSF = classical least squares filter
SF = sequential filter
Optimum *SF* = sequential filter which accurately models the spacecraft environment and data equations

Subscripts and Superscripts
R, X, Y = the spacecraft roll, spin, yaw axes, respectively
$(\,)^T$ = transpose of matrix in brackets

Received December 6, 1972; revision received September 6, 1973.
Index categories: Navigation, Control, and Guidance Theory; Spacecraft Navigation, Guidance, and Flight-Path Control.

* Senior Engineer.
† Engineer.

Introduction

THE navigation of interplanetary spacecraft is degraded by unmodeled, random nongravitational forces affecting the spacecraft. Major sources of these random forces have been variations in solar pressure, leakage from attitude control jets, and fluctuations in solar wind. Unmodeled accelerations, commonly referred to as process noise, generally produce negligible perturbations on the actual spacecraft trajectory. However their effect on conventional Earth-based radio tracking data, such as two-way Doppler and ranging, can severely limit the estimation accuracies attainable with a classical least squares filter.[1,2]

Estimation difficulties caused by process noise can be alleviated by the application of a new data type called difference-*QVLBI*.[3] The ultimate solution to the problem, however, is an optimal sequential filter that precisely models the random process. Several modified Kalman filters have been designed which assume that random accelerations can be described by a first-order Gauss-Markov process.[4,5] Although this model may adequately represent major sources of process noise, suboptimal filtering still occurs when imprecise parameters defining the process are assumed. It is desirable therefore to evaluate filtering sensitivity to these mismodeled parameters. Nishimura,[6] Griffin and Sage[7] and others have investigated this kind of sensitivity for continuous and discrete Kalman filters.

Numerical difficulties present in conventional Kalman filtering algorithms when dealing with poorly conditioned problems have generated increased interest in the application of Householder techniques to linear least squares estimation.[8] By utilizing Householder transformations it is possible to avoid the formation and inversion of a near singular normal matrix. Instead, the square-root of the normal, or information, matrix is employed. Dyer and McReynolds extended this square-root filtering technique to include process noise.[9] For numerical reasons then it is desirable to construct square-root evaluation algorithms to accompany these computationally superior square-root filters. Furthermore, the square-root derivation of filtering and evaluation equations results in simplifications which allow

this approach to be more flexible and less unwieldy than conventional Kalman derivations.

In this paper an algorithm is derived for evaluating the performance of a square-root filter which inexactly models process noise as a first-order Gauss-Markov sequence. The algorithm is then applied to analyze the relative merits of several tracking data and filtering strategies for an interplanetary mission.

Sequential Filter and Evaluation Algorithm

The primary source of random, nongravitational forces acting on a Mariner-type spacecraft is leakage from the attitude control jets. These jets are oriented in three orthogonal directions along the spacecraft roll, pitch, and yaw (R, X, Y) axes. Leakage of gas from one of these valves produces a slowly varying acceleration along the corresponding axis. Therefore, the random process affecting the spacecraft can be approximated by three orthogonal, piecewise constant accelerations along the R, X, and Y axes. These accelerations are assumed to be uncorrelated with one another but to have autocorrelations which are exponential in time. In this sense the process is represented by a first-order Gauss-Markov sequence with zero mean. Hence this process is given by

$$p_{i+1} = Mp_i + w_i \tag{1}$$

$$M = \text{diag}(m_R, m_X, m_Y) \tag{2}$$

$$m_R = \exp[-\Delta t/\tau_R] \tag{3}$$

The diagonals m_X and m_Y are obtained from Eq. (3) when R is replaced by X and Y, respectively

$$\Delta t = t_{i+1} - t_i \tag{4}$$

Since the intervals $(t_{i+1} - t_i)$ are assumed to be equal for all i, the matrix M is constant.

The vector w_i represents a random perturbation to the process which has the following properties:

$$E[w_i] = 0 \tag{5}$$

$$E[p_i w_i^T] = 0 \tag{6}$$

$$E[w_i w_j^T] = \delta_{ij}\Lambda_w \tag{7}$$

The symbol δ_{ij} denotes a Kronecher delta and $E[\ ]$ indicates an ensemble average. In order for the process to be stationary, the covariance Λ_w is constrained in the following way:

$$\Lambda_w = (I - M^2)\Lambda_p \tag{8}$$

where

$$\Lambda_p = E[p_i p_i^T] = \begin{bmatrix} \sigma_R{}^2 & & 0 \\ & \sigma_X{}^2 & \\ 0 & & \sigma_Y{}^2 \end{bmatrix} \tag{9}$$

A sequential filter which employs this process noise model provides a more optimal means of analyzing data from a noisy spacecraft than does a classical least squares filter. A detailed description of such a sequential filter, in square-root form, is given in Ref. 5. The more essential equations are repeated here in order to develop an algorithm for evaluating the filter's sensitivity to mismodeling of the process noise.

For a linear, discrete system, the state transition equation for the parameter vector $y(n \times 1)$ and the equation for the observable $z(m \times 1)$ are

$$y_{i+1} = \phi_{i+1,i}\, y_i + Gw_i \tag{10}$$

$$z_i = A_i y_i + n_i \tag{11}$$

where w_i and n_i are independent and have zero mean.

Therefore

$$E[w_i n_j^T] = 0 \tag{12}$$

Also,

$$E[n_i n_j^T] = \delta_{ij} I \tag{13}$$

and again,

$$E[w_i w_j^T] = \delta_{ij}\Lambda_w$$

The assumption of unit measurement noise in Eq. (13) results in no loss of generality. It simply implies Eq. (11) has been appropriately scaled.

The matrices $\phi_{i+1,i}$ and A_i are computed from a nominal trajectory, and hence each y_i is a correction to the nominal state at that time.

If the accelerations p_i are included as estimated parameters, then y_i can be partitioned such that

$$y_i = \begin{bmatrix} \lambda_i \\ p_i \end{bmatrix} \tag{14}$$

Hence

$$\phi_{i+1,i} = \begin{bmatrix} U_{i+1,i} & V_{i+1,i} \\ 0 & M \end{bmatrix} \tag{15}$$

and

$$G = \begin{bmatrix} 0 \\ I \end{bmatrix} \tag{16}$$

A priori estimates of y_i are referred to as $\tilde{y}_i$ and the corresponding covariance as $\tilde{\Lambda}_i$. These estimates can be included as data by the following:

$$\tilde{z}_i = \tilde{\Lambda}_i{}^{-1/2} y_i + \tilde{n}_i \tag{17}$$

where $\tilde{y}_i = \tilde{\Lambda}_i{}^{1/2}\tilde{z}_i$

$$E[\tilde{n}_i] = 0 \tag{18}$$

$$E[\tilde{n}_i \tilde{n}_i^T] = I \tag{19}$$

In square-root form, a weighted least squares estimate of y_i is that vector $\hat{y}_i$ which minimizes the quantity

$$v = \left\| \begin{bmatrix} \tilde{\Lambda}_i{}^{-1/2} \\ A_i \end{bmatrix} \hat{y}_i - \begin{bmatrix} \tilde{z}_i \\ z_i \end{bmatrix} \right\| \tag{20}$$

A Householder transformation Q is constructed such that $Q^T Q = I$ and

$$Q \begin{bmatrix} \tilde{\Lambda}_i{}^{-1/2} \\ A_i \end{bmatrix} = \begin{bmatrix} R_i \\ 0 \end{bmatrix} \tag{21}$$

where R_i is upper triangular.[8] Let

$$Q \begin{bmatrix} \tilde{z}_i \\ z_i \end{bmatrix} = \begin{bmatrix} z_i' \\ * \end{bmatrix}^{\ddagger} \tag{22}$$

Then the quantity v is minimized when

$$\hat{y}_i = R_i{}^{-1} z_i' \tag{23}$$

The vector z_i' is given by

$$z_i' = R_i y_i + n_i' \tag{24}$$

where

$$n_i' = Q_1 \begin{bmatrix} \tilde{n}_i \\ n_i \end{bmatrix} \tag{25}$$

and Q_1 represents the first n rows of the matrix Q. Hence from Eqs. (23) and (24)

$$E[\hat{y}_i] = y_i \tag{26}$$

$$\Lambda_i = E[(\hat{y}_i - y_i)(\hat{y}_i - y_i)^T] = R_i{}^{-1} R_i{}^{-1T} \tag{27}$$

In order to add data at t_{i+1}, it is necessary to map to t_{i+1} via Eq. (10).

Let

$$\tilde{y}_{i+1} = \phi_{i+1,i}\hat{y}_i \tag{28}$$

and

$$\tilde{\Lambda}_{i+1} = \phi_{i+1,i}\Lambda_i \phi_{i+1,i}^T + G\Lambda_W G^T \tag{29}$$

The covariance, $\tilde{\Lambda}_{i+1}$, is factored such that

$$\tilde{\Lambda}_{i+1} = \phi_{i+1,i} R_i{}^{-1}[I + B_i \Lambda_W B_i^T] R_i{}^{-1T} \phi_{i+1,i}^T \tag{30}$$

where§

$$B_i = -R_i \phi_{i+1,i}^{-1} G \tag{31}$$

A Householder transformation P can be constructed such that

‡ The symbol * denotes a nonzero vector which is unused and hence unnamed.

§ The existence of $\phi_{i+1,i}^{-1}$ is assumed here and discussed later.

$$P\begin{bmatrix} I \\ \Lambda_w^{1/2} B_i^T \end{bmatrix} = \begin{bmatrix} R_{yw}^T \\ 0 \end{bmatrix} \tag{32}$$

Then

$$\tilde{\Lambda}_{i+1}^{-1/2} = R_{yw}^{-1} R_i \phi_{i+1,i}^{-1} \tag{33}$$

Hence, the a priori data equations at t_{i+1} are obtained by applying Eq. (10) to Eq. (24) and premultiplying by R_{yw}^{-1}. These equations are given by

$$\tilde{z}_{i+1} = [R_{yw}^{-1} R_i \phi_{i+1,i}^{-1}] y_{i+1} + \tilde{n}_{i+1} \tag{34}$$

where

$$\tilde{z}_{i+1} = R_{yw}^{-1} z_i' \tag{35}$$

and

$$\tilde{n}_{i+1} = R_{yw}^{-1}[n_i' + B_i w_i] \tag{36}$$

From the definition of R_{yw}, it is clear that $\tilde{n}_{i+1}$ has unit covariance as assumed in Eq. (19).

If (i) is replaced by $(i+1)$ in Eq. (20) and data are added, another Householder transformation can be constructed, etc., until the entire data arc is processed.

To the extent that Eqs. (10–16) faithfully represent the true environment, the filter is optimum and $\hat{y}_i$ in Eq. (23) is the minimum variance estimate of y_i. However, it is desirable to evaluate the errors in $\hat{y}_i$ when the random process is mismodeled by the filter.

Let the "true" or "actual" process be given by

$$\bar{p}_{i+1} = \bar{M}\bar{p}_i + \bar{w}_i \tag{37}$$

$$\bar{M} = (\bar{m}_R, \bar{m}_X, \bar{m}_Y) \tag{38}$$

$$\bar{m}_R = \exp[-\Delta t/\bar{\tau}_R] \tag{39}$$

Let

$$E[\bar{p}_i \bar{p}_i^T] = \bar{\Lambda}_p \tag{40}$$

$$E[\bar{w}_i \bar{w}_j^T] = \delta_{ij} \bar{\Lambda}_w \tag{41}$$

and

$$\bar{\Lambda}_w = (I - \bar{M}^2)\bar{\Lambda}_p \tag{42}$$

The filter's performance will be evaluated for the case where the correlation times (τ_R, τ_X, τ_Y) and sigmas (σ_R, σ_X, σ_Y) of the process noise are mismodeled.

If the actual process is given by Eq. (37) then the correct state transition equation is

$$\bar{y}_{i+1} = \bar{\phi}_{i+1,i} \bar{y}_i + G\bar{w}_i \tag{43}$$

where

$$\bar{\phi}_{i+1,i} = \begin{bmatrix} U_{i+1,i} & V_{i+1,i} \\ 0 & \bar{M} \end{bmatrix} \tag{44}$$

If Eqs. (43) and (44) are compared to the assumed Eqs. (10) and (15) it is clear that the actual and assumed state transition equations are identical except for the matrix M and the white noise w_i. Furthermore, it is important to note that the existence of both $\phi_{i+1,i}^{-1}$ and $\bar{\phi}_{i+1,i}^{-1}$ is assured if M and $\bar{M}$ are each positive definite.

Let the actual data equation at t_1, corresponding to the assumed Eqs. (24), be given by

$$z_i' = \bar{R}_i y_i + n_a(i) \tag{45}$$

Mapping to t_{i+1} with Eq. (43) and premultiplying by R_{yw}^{-1} to get the actual $\tilde{z}_{i+1}$, we have

$$\tilde{z}_{i+1} = R_{yw}^{-1} z_i' = [R_{yw}^{-1} \bar{R}_i \bar{\phi}_{i+1,i}^{-1}] y_{i+1} + \tilde{n}_a(i+1) \tag{46}$$

where

$$\tilde{n}_a(i+1) = R_{yw}^{-1}[n_a(i) + \bar{B}_i \bar{w}_i] \tag{47}$$

and

$$\bar{B}_i = -\bar{R}_i \bar{\phi}_{i+1,i}^{-1} G \tag{48}$$

When data at t_{i+1} are included and the assumed array in the filter is triangularized by a Householder transformation $Q(i+1)$, the filter then assumes

$$z_{i+1}' = R_{i+1} y_{i+1} + n_{i+1}' \tag{49}$$

where z_{i+1}', R_{i+1} and n_{i+1}' are defined by Eqs. (22), (21), and (25), respectively.

However, if $Q(i+1)$ is applied to the actual data equations then z_{i+1}' is given by

$$z_{i+1}' = \bar{R}_{i+1} y_{i+1} + n_a(i+1) \tag{50}$$

where $\bar{R}_{i+1}$ and $n_a(i+1)$ are defined by

$$Q(i+1)\begin{bmatrix} R_{yw}^{-1} \bar{R}_i \bar{\phi}_{i+1,i}^{-1} \\ A_{i+1} \end{bmatrix} = \begin{bmatrix} \bar{R}_{i+1} \\ * \end{bmatrix} \tag{51}$$

and

$$Q(i+1)\begin{bmatrix} \tilde{n}_a(i+1) \\ n_{i+1} \end{bmatrix} = \begin{bmatrix} n_a(i+1) \\ * \end{bmatrix} \tag{52}$$

When the vector y_{i+1} is estimated by the filter to be

$$\hat{y}_{i+1} = R_{i+1}^{-1} z_{i+1}' \tag{53}$$

the actual errors in $\hat{y}_{i+1}$ are obtained by substituting Eq. (50) into Eq. (53).

Hence

$$\hat{y}_{i+1} - y_{i+1} = R_{i+1}^{-1}\{[\bar{R}_{i+1} - R_{i+1}] y_{i+1} + n_a(i+1)\} \tag{54}$$

Let R_{i+1} be partitioned as follows

$$R_{i+1} = \begin{bmatrix} R_\lambda & R_{\lambda p} \\ 0 & R_p \end{bmatrix}_{i+1} \tag{55}$$

From Eqs. (21) and (33) which define R_{i+1}, and from Eqs. (44) and (51), it is clear that $\bar{R}_{i+1}$ has the form

$$\bar{R}_{i+1} = \begin{bmatrix} R_\lambda & \bar{R}_{\lambda p} \\ 0 & \bar{R}_p \end{bmatrix}_{i+1} \tag{56}$$

That is, if the initial a priori covariance $\tilde{\Lambda}_o$ assumed by the filter is identical to the "actual" a priori covariance except for the last three columns (which correspond to the a priori information on p_o), then R_{i+1} and $\bar{R}_{i+1}$ are similarly related for all i.

Hence

$$\hat{y}_{i+1} - y_{i+1} = R_{i+1}^{-1}\{D_{i+1} p_{i+1} + n_a(i+1)\} \tag{57}$$

where

$$D_{i+1} = \begin{bmatrix} \bar{R}_{\lambda p} \\ \bar{R}_p \end{bmatrix}_{i+1} - \begin{bmatrix} R_{\lambda p} \\ R_p \end{bmatrix}_{i+1} \tag{58}$$

Let

$$\xi_{i+1} = n_a(i+1) + D_{i+1} p_{i+1} \tag{59}$$

Then the actual covariance of $\hat{y}_{i+1}$ for the process described by Eqs. (37–42) is given by

$$\bar{\Lambda}_{i+1} = R_{i+1}^{-1} \Lambda_\xi R_{i+1}^{-1T} \tag{60}$$

where

$$\Lambda_\xi = E[\xi_{i+1} \xi_{i+1}^T] \tag{61}$$

When $\bar{M} \equiv M$ and $\bar{\Lambda}_p \equiv \Lambda_p$, then $\Lambda_\xi = I$ and the actual covariance reduces to the minimum variance computed by the filter in Eq. (27).

Equations for the covariance, Λ_ξ, of the effective data errors are given in the Appendix.

Application

This algorithm for determining filter sensitivity to mismodeled process noise was applied to the analysis of three tracking data schemes for an interplanetary mission. As seen from the trajectory in Fig. 1, the spacecraft is launched from Earth on Oct. 24, 1973, and encounters Venus on Feb. 4, 1974. It is this portion of the trajectory for which the analysis was performed. Using Earth-based tracking data acquired during the month preceding Venus encounter, the filter estimated the approach trajectory at Venus. The accuracy of an estimate was then described by a 1σ miss ellipse in the B-plane at Venus.[10] This miss ellipse can be thought of as a measure of the two-dimensional position uncertainties at encounter, independent of the arrival time.

The data arc begins on Jan. 1, 1973, and continues for 32 days until Feb. 2, 1974. Doppler and range data were simulated for three widely separated tracking stations in the

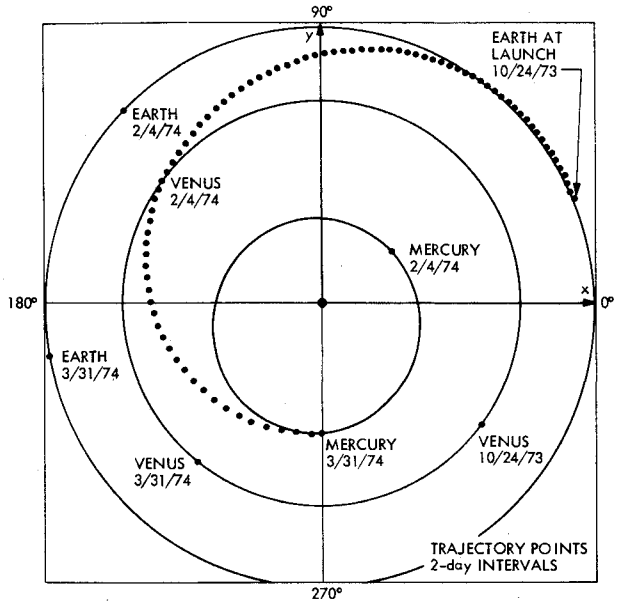

Fig. 1 Projection of heliocentric trajectory in ecliptic plane.

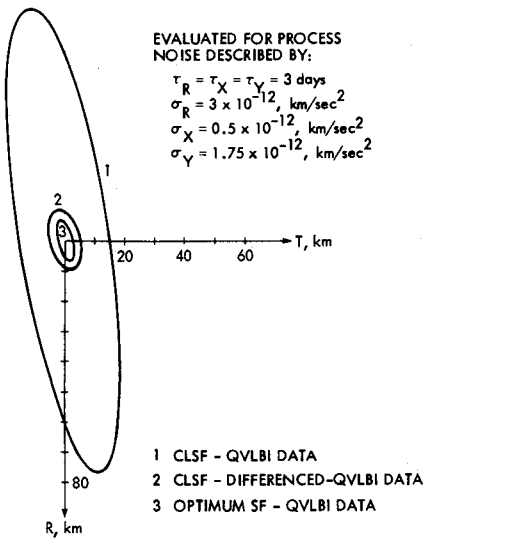

Fig. 3 *B*-plane miss ellipses at Venus for a typical random environment.

Deep Space Network. The tracking pattern for a typical 24-hour period is illustrated in Fig. 2. While Doppler measurements were taken every hour, only one ranging point was obtained during each pass over a station. As shown in Fig. 2 each station receives Doppler data simultaneously with at least one other station during a day. Range measurements from DSS 42 and DSS 14 are nearly simultaneous. When two widely separated tracking stations receive simultaneous, or nearly simultaneous, signals the data are referred to as quasi-very-long baseline interferometry (*QVLBI*). The attractive feature of *QVLBI* data types is realized when the simultaneous data are explicitly differenced. The resulting differenced-data type is particularly valuable when an unmodeled random process affects the spacecraft. By differencing the data one greatly reduces that portion of the signal which produces large estimation errors in classical least squares filtering.[3] However, when *QVLBI* data types are explicitly differenced, the process noise problem is ameliorated at the expense of eliminating geocentric range and range rate information in the data. This information can be retained to some extent by including very loosely weighted conventional data as well as the differenced-*QVLBI*.

In this study the estimation accuracies for three data strategies were compared. These strategies are defined by the following characteristics.

1) All the data taken during the 32 days of tracking were included. The Doppler data were given weights of 1 mm/sec for a 60 sec count time, and a sample rate of one point per minute. Range data were assumed accurate to 50 m. Data strategy No. 1 is referred to as "*QVLBI*."

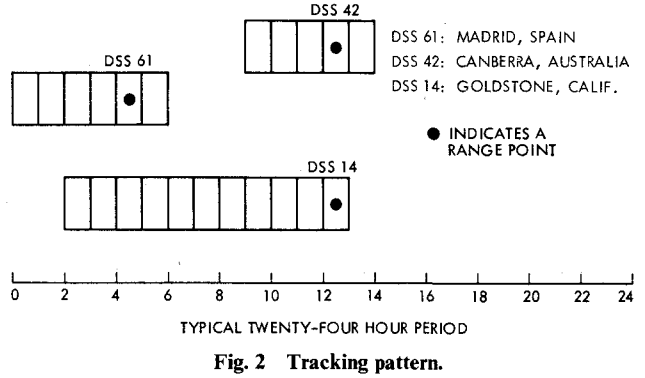

Fig. 2 Tracking pattern.

2) All the simultaneous, or nearly simultaneous, Doppler and range data in strategy No. 1 were explicitly differenced to create two new data types which were assigned the same weights as the Doppler and range in No. 1. Conventional data were retained from all the stations but assigned weights which were a factor of 500 larger than the differenced data. This strategy is referred to as "Differenced-*QVLBI*."

3) The third data strategy is identical to No. 1, except that all data from DSS 14 were eliminated. Therefore, no simultaneous measurements occur.

For each of these data strategies estimation accuracies were computed—for both the classical least squares and the sequential filtering techniques, and in the presence of process noise. The process noise was represented by Eq. (1), where the most likely values for the parameters were assumed to be

$$\begin{aligned} \sigma^R &= 3 \times 10^{-12}\ \text{km/sec}^2 \\ \sigma_X &= 0.5 \times 10^{-12}\ \text{km/sec}^2 \\ \sigma_Y &= 1.75 \times 10^{-12}\ \text{km/sec}^2 \\ \tau^R &= \tau_X = \tau_Y = 3\ \text{days} \end{aligned} \tag{62}$$

Estimated parameters included the spacecraft state and the three accelerations, p_R, p_X, p_Y. Since the classical least squares filter contains no model for random accelerations, it estimates p_R, p_X, and p_Y to be constant over the entire data interval. A priori uncertainty in the spacecraft state was assumed to be 10,000 km and 1 km/sec in each component of position and velocity, respectively.

Results of Analysis

The *B*-plane miss ellipses shown in Fig. 3 demonstrate the vastly different accuracies obtained for various filter-data strategy configurations. Uncertainties were computed assuming a random environment described by Eq. (62). As seen in Fig. 3, the classical least squares filter (*CLSF*), employing *QVLBI* data, produces a 1σ miss ellipse with a semimajor axis of 78 km. However, if the same filter analyzes Differenced-*QVLBI* data the semimajor axis reduces to 11 km. Ellipse No. 3 represents uncertainties from the sequential filter (*SF*) which accurately models the process and uses *QVLBI* data. It has a semimajor axis of 7 km.

Results similar to those given in Fig. 3 are presented in Figs. 4 and 5, where the 1σ uncertainty in the process noise (σ_p) is allowed to vary from 10^{-13} to 10^{-10} km/sec^2. In Fig. 4 the semimajor axis of the miss ellipse (*SMA*) is plotted vs σ_p for four strategies. Figure 5 shows the corresponding results for the semiminor axis (*SMI*). Together, these figures

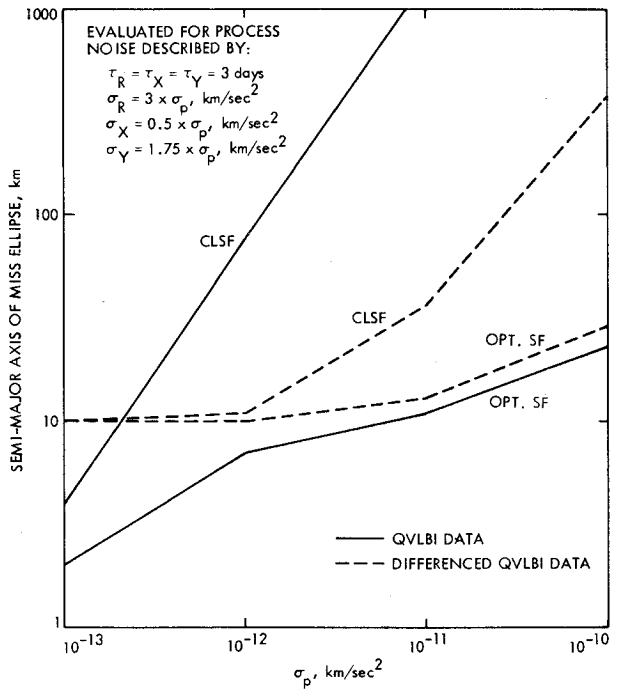

Fig. 4 Semimajor axis of miss ellipse vs process noise.

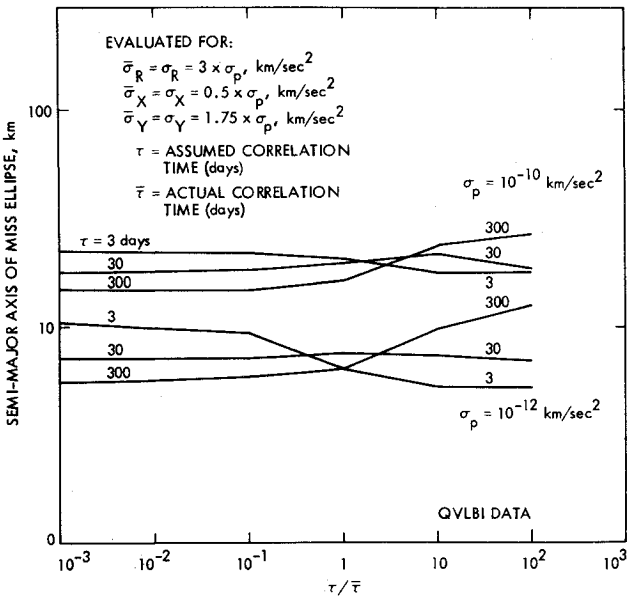

Fig. 6 Sensitivity to mismodeling of correlation times.

illustrate the relative merits of *QVLBI* and Differenced-*QVLBI* data types. When σ_p is less than 10^{-12} km/sec^2 the *CLSF* and the optimum sequential filter, using Differenced-*QVLBI* data, attain about the same level of accuracy. However as the level of process noise becomes greater than 10^{-12} km/sec^2, the optimum sequential filter produces much more accurate estimates than the *CLSF*. Furthermore, for all levels of process noise when an optimum sequential filter is employed, results using *QVLBI* and Differenced-*QVLBI* data are nearly identical. This is demonstrated by the lower two curves in Figs. 4 and 5.

It is also apparent from these figures that some information available in *QVLBI* data is lost when the simultaneous signals are explicitly differenced. As σ_p reduces to 10^{-13} km/sec^2, *SMA* decreases to 2 km when the sequential filter employs *QVLBI* data. However, the same filter using Differenced-*QVLBI* data produces an *SMA* of 10 km, the same value obtained for $\sigma_p = 10^{-12}$ km/sec. In fact, both curves representing Differenced-*QVLBI* data level off at *SMA* = 10 km for $\sigma_p = 10^{-12}$ km/sec^2, while the two curves obtained by using *QVLBI* data continue downward as σ_p decreases.

For all levels of process noise, the sequential filter with *QVLBI* data appears to be the most attractive choice, with sequential filtering of Differenced-*QVLBI* next. However, the results in Figs. 3–5 were obtained by assuming that the sequential filter modeled the random process correctly. To complete the analysis it is necessary to determine how sensitive the sequential filter results are to mismodeling of the process noise. Therefore, the evaluation algorithm described in this paper was applied to compute the "actual" *B*-plane uncertainties from the sequential filter when the following type of mismodeling occurs.

1) Only the 1σ uncertainty, σ_p, is mismodeled where,

$$\sigma_R = 3 \times \sigma_p (\text{km/sec}^2)$$
$$\sigma_X = 0.5 \times \sigma_p (\text{km/sec}^2)$$
$$\sigma_Y = 1.75 \times \sigma_p (\text{km/sec}^2)$$

2) The σ are correct but the correlation time, τ, is mismodeled where $\tau_R = \tau_X = \tau_Y = \tau$.

Figures 6–9 illustrate filtering sensitivity to mismodeled process noise for the three data strategies studied. The semimajor axis of the actual *B*-plane ellipse is plotted versus the ratio of assumed to actual σ_p (or τ) for several fixed values of the assumed parameter. Although it was more convenient for this particular application to display results for fixed values of the assumed parameters, it is often preferable to fix the actual and vary the assumed. If this latter approach were taken each curve would then attain a minimum where the actual and assumed are equal.

In Fig. 6 the semimajor axis of the actual *B*-plane ellipse is plotted as a function of $\tau/\bar{\tau}$ where τ is the correlation time assumed by the filter and $\bar{\tau}$ is the actual correlation time. The top group of three curves displays sensitivities to mismodeling of τ when $\sigma_p = 10^{-10}$ km/sec^2, while the lower group represents the case where $\sigma_p = 10^{-12}$ km/sec^2. It is immediately obvious from this figure that errors of several orders of magnitude in assumed correlation times do not significantly hinder the sequential filter. Notice for $\sigma_p = 10^{-10}$ km/sec^2 when the filter assumes a correct correlation time of 300 days ($\tau/\bar{\tau} = 1$) the *SMA* is 16 km. If the actual correlation time is 3 days ($\tau/\bar{\tau} = 100$) then the *SMA* increases to 27 km.

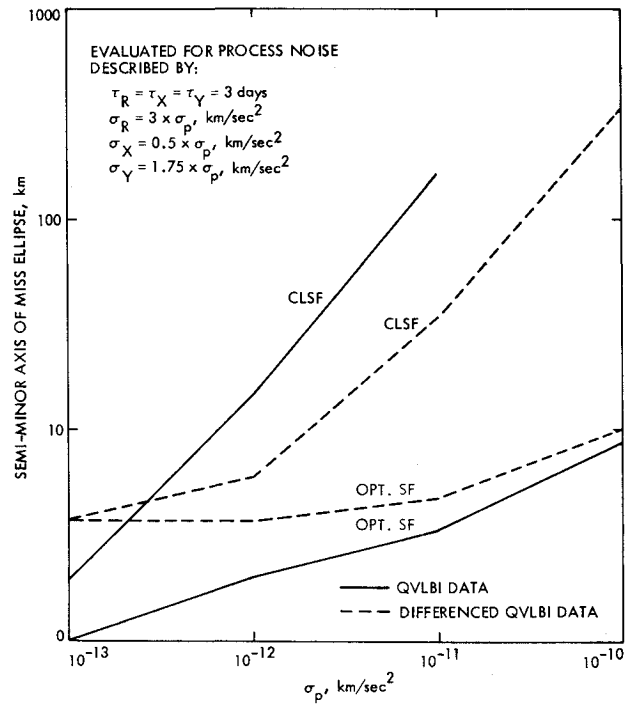

Fig. 5 Semiminor axis of miss ellipse vs process noise.

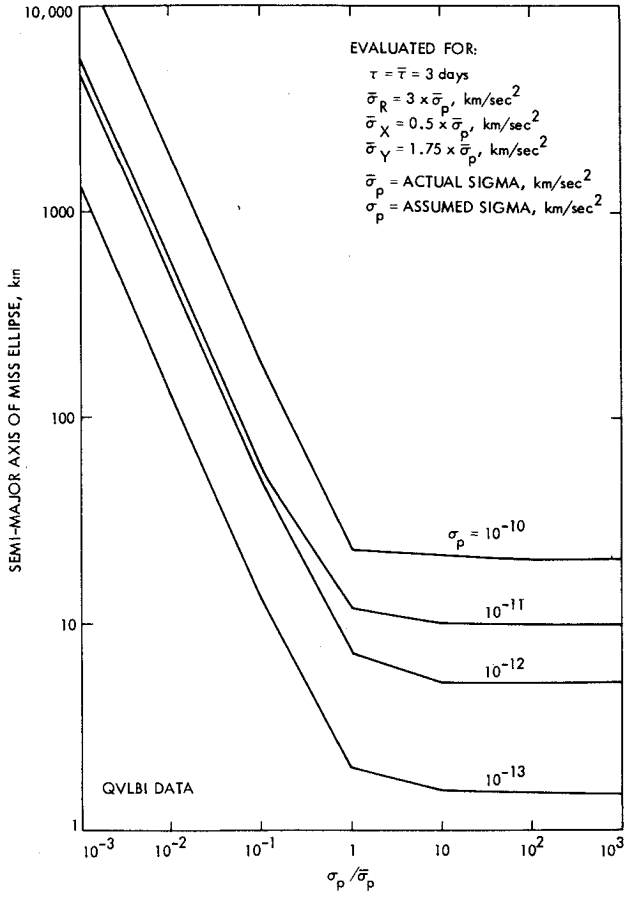

Fig. 7 Sensitivity to mismodeled σ—with *QVLBI* data.

Before sensitivities to mismodeled correlation times are dismissed as relatively insignificant one should note that when τ approaches infinity the sequential filter assumes the process is represented by constant accelerations. Hence, in the limit as $\tau \to \infty$ the sequential filter accuracies are identical to those of the *CLSF*. On the other hand, it is clear that there exists some minimum value for an intelligent choice of τ. As $\tau \to 0$ the matrix M becomes non-negative definite and the accelerations can no longer be estimated. For this particular analysis, one might assume $\tau = 30$ to minimize filter sensitivity to this parameter.

Although the sequential filter shows little sensitivity to mismodeling of correlation times, the same cannot be said about mismodeled sigmas of the process noise. The results in Fig. 7 illustrate sensitivities to mismodeled σ when *QVLBI* data are analyzed by the sequential filter. In this figure the semimajor axis of the actual miss ellipse is plotted as a function of the ratio $\sigma_p/\bar{\sigma}_p$. The 1σ uncertainty assumed by the sequential filter is σ_p while $\bar{\sigma}_p$ denotes the actual sigma of the process noise. Results are plotted for constant values of σ_p. For the case where $\sigma_p = 10^{-12}$ km/sec^2 and $\sigma_p/\bar{\sigma}_p = 1.$, the semimajor axis is 7 km. This is the optimal filtering result noted previously from Figs. 3 and 4. Notice that if the actual process has a σ of 10^{-11} km/sec^2 ($\sigma_p/\bar{\sigma}_p = 0.1$) then the actual *SMA* is 50 km. However if the filter assumed $\sigma_p = \bar{\sigma}_p = 10^{-11}$ km/sec^2, then for $\sigma_p/\bar{\sigma}_p = 1$ on that curve the optimal *SMA* is 12 km.

Similar results are shown in Fig. 8 for the case where Differenced-*QVLBI* data are used. By comparing Figs. 7 and 8 it is possible to determine which data strategy is preferable when this type of mismodeling occurs. Notice that in Fig. 8 all curves lie above *SMA* = 10 km whereas in Fig. 7 the curves for $\sigma_p = 10^{-12}$ km/sec^2 and $\sigma_p = 10^{-13}$ km/sec^2 both fall below 10 km when the filter assumes $\sigma_p \geqq \bar{\sigma}_p$. This comparison is another illustration of the loss of some geocentric information when simultaneous data are differenced. Also by comparing Figs. 7 and 8 we see that the curves for $\sigma_p = 10^{-10}$ and $\sigma_p = 10^{-11}$ km/sec^2 are nearly identical for each data type. However the curves for $\sigma_p = 10^{-12}$ and $\sigma_p = 10^{-13}$ in Fig. 8 show slightly less sensitivity to mismodeling than the corresponding curves in Fig. 7. Hence if the filter, using *QVLBI* data assumed $\sigma_p = 10^{-13}$ km/sec^2 but actually $\bar{\sigma}_p = 10^{-11}$ then the actual *SMA* is 130 km. However when Differenced-*QVLBI* data are used, Fig. 8 shows that for this type of modeling error *SMA* = 20 km.

By comparing Figs. 7 and 8 one could conclude:

1) If the assumed σ_p is 10^{-11} or 10^{-10} km/sec^2 nothing is gained by using Differenced-*QVLBI* instead of *QVLBI*.

2) If the assumed $\sigma_p = 10^{-12}$ km/sec^2 and actual $\bar{\sigma}_p < 3 \times 10^{-12}$, or if assumed $\sigma_p = 10^{-13}$ and actual $\bar{\sigma}_p < 10^{-12}$ the same conclusion applies.

3) However, if assumed $\sigma_p \leqq 10^{-12}$ and actual $\bar{\sigma}_p \geqq 10^{-11}$ the Differenced-*QVLBI* data type is preferable.

Notice, however, that by assuming $\sigma_p = 10^{-11}$ km/sec^2 and using *QVLBI* data, one obtains *SMA* = 10 km for any actual $\bar{\sigma}_p \geqq 10^{-11}$. But 10 km is the minimum *SMA* attainable with Differenced-*QVLBI* data, regardless of the modeling. Hence, for this particular study if sequential estimation is performed with *QVLBI* data and with an assumed $\sigma_p = 10^{-11}$ km/sec^2, the need for Differenced-*QVLBI* can be dismissed.

Thus far nothing has been said about data strategy No. 3 which contains no simultaneous data. Since much additional effort is expended to obtain the simultaneous data contained in *QVLBI* data, it is worthwhile to investigate estimation accuracies attainable when conventional (nonoverlapping) data types are employed. Figure 9 illustrates the sensitivity of sequential filtering with data strategy No. 3 to mismodeled process noise. This figure has a striking similarity to Fig. 7. Although all curves in Fig. 9 are slightly above the corresponding curves in Fig. 7, the shift appears to be due primarily to the differences in the total number of observations included. By comparing these figures one can

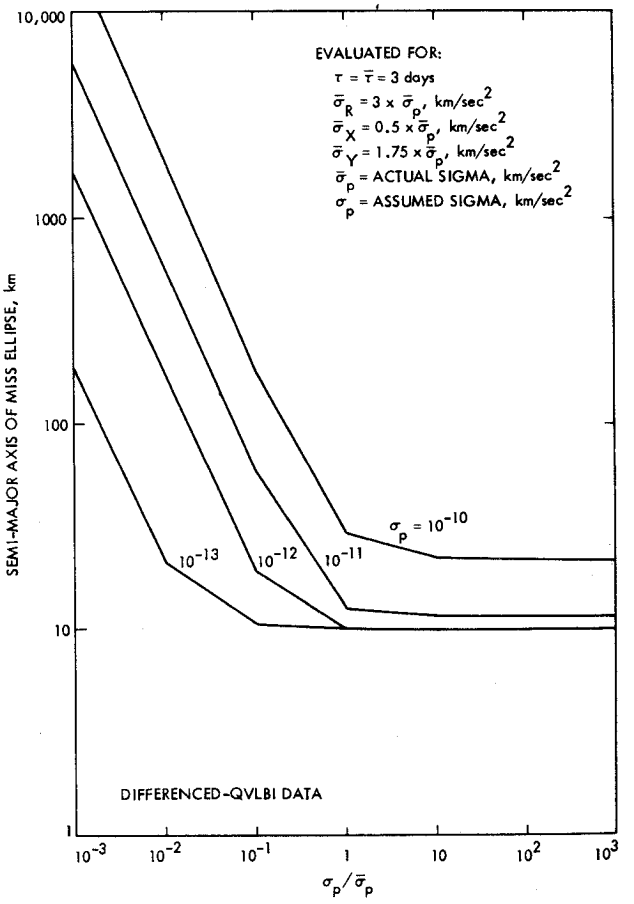

Fig. 8 Sensitivity to mismodeled σ—with Differenced-*QVLBI* data.

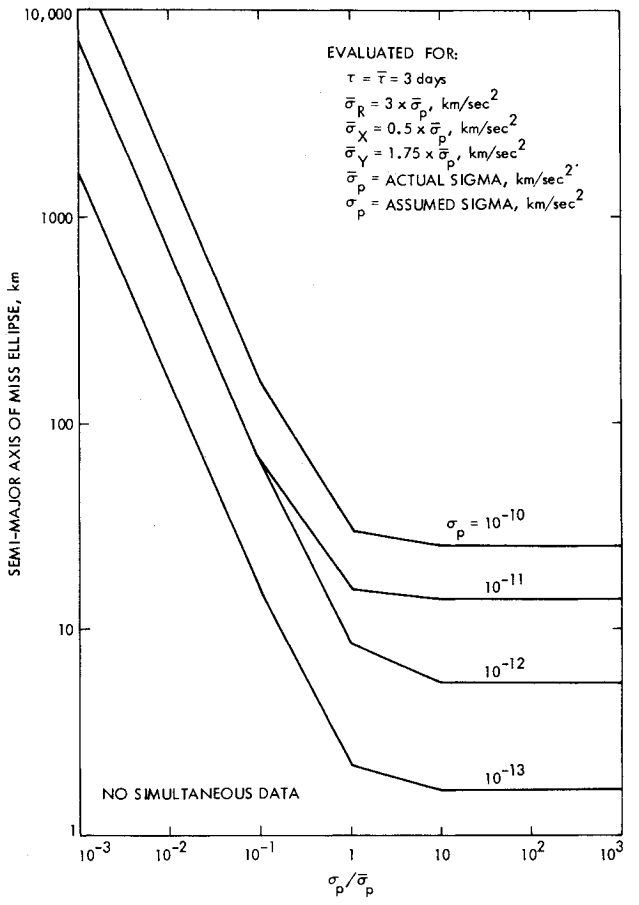

Fig. 9 Sensitivity to mismodeled σ—with no simultaneous data.

conclude that very little information is lost when simultaneous data are omitted.

Sensitivities of the semiminor axis (*SMI*) to mismodeled process noise display the same characteristics noted in Figs. 7–9 for the semimajor axis.

This analysis is one example of how the evaluation algorithm can be applied. In this particular analysis, the Earth-spacecraft distance was less than 1 AU. For greater distances, process noise effects on estimation accuracies are magnified. Furthermore, the gravitational influence of a third body (the sun) also diminished the difficulties with process noise in this study. For other missions, such as an outer planet fly-by, a study similar to this one may produce entirely different results and conclusions.

Conclusions

An algorithm for evaluating the sensitivity of a sequential filter to mismodeled process noise has been formulated. A computer program incorporating this algorithm, provides sequential filtering and evaluation in a numerically efficient, square-root form. This program can be readily applied to the analysis of optimum filtering and tracking strategies for interplanetary missions.

Appendix

The computation of Λ_ξ directly from Eq. (59) gives

$$\Lambda_\xi(i+1) = \Lambda_n(i+1) + D_{i+1}\bar{\Lambda}_p D_{i+1}^T + \Lambda_{np}(i+1)D_{i+1}^T + D_{i+1}\Lambda_{np}^T \tag{A1}$$

where

$$\Lambda_n(i+1) = E[n_a(i+1)n_a(i+1)^T] \tag{A2}$$

and

$$\Lambda_{np}(i+1) = E[n_a(i+1)p_{i+1}^T] \tag{A3}$$

This formula for Λ_ξ is not difficult analytically. However, since the cross covariance Λ_{np} can become quite large, calculation of Λ from Eq. (A1) is numerically inappropriate. Computational difficulties are alleviated if analytic cancellations inherent in Eq. (59) are performed. Hence we can write

$$\xi_{i+1} = K_{i+1}[\xi_i + B_i(\bar{M}-M)p_i + B_i w_i] + Q_{12}n_{i+1} \tag{A4}$$

where

$$K_{i+1} = Q_{11}(i+1)R_{yw}^{-1}(i) \tag{A5}$$

The Householder transformation $Q(i+1)$ has been partitioned so that

$$Q(i+1) = \begin{bmatrix} Q_{11} & Q_{12} \\ Q_{21} & Q_{22} \end{bmatrix}_{i+1} \tag{A6}$$

Equation (A4) for ξ_{i+1} is obtained by substituting in Eq. (59) for $n_a(i+1)$ and p_{i+1}, applying Eqs. (52, 47, and 37), and by using the identities

$$D_{i+1} = K_{i+1}(B_i - \bar{B}_i) \tag{A7}$$

and

$$(B_i - \bar{B}_i)\bar{M} = B_i(\bar{M}-M) + D_i \tag{A8}$$

These identities follow from definitions of B_i and $\bar{B}_i$, Eqs. (31 and 48), and from Eqs. (21, 51, and 58) which prove (A7).

Rewrite Eq. (A4) in the following way

$$\xi_{i+1} = Q_1(i+1)\begin{bmatrix} c_{i+1} \\ n_{i+1} \end{bmatrix} \tag{A9}$$

where

$$Q_1 = [Q_{11}Q_{12}] \tag{A10}$$

$$\varepsilon_{i+1} = H_{i+1}\begin{bmatrix} \xi_i \\ p_i \\ w_i \end{bmatrix} \tag{A11}$$

and

$$H_{i+1} = R_{yw}^{-1}(i)[I \vdots B_i(\bar{M}-M) \vdots B_i] \tag{A12}$$

Then

$$\Lambda_\xi(i+1) = Q_1(i+1)\begin{bmatrix} \Lambda_\varepsilon & 0 \\ 0 & I \end{bmatrix} Q_1^T(i+1) \tag{A13}$$

where

$$\Lambda_\varepsilon = H_{i+1}\begin{bmatrix} \Lambda_\xi(i) & \Lambda_{\xi p}(i) & 0 \\ \Lambda_{\xi p}^T(i) & \bar{\Lambda}_p & 0 \\ 0 & 0 & \bar{\Lambda}_w \end{bmatrix} H_{i+1}^T \tag{A14}$$

From Eq. (A4) it is clear that

$$\Lambda_{\xi p}(i) = E[\xi_i p_i^T] = K_i[\Lambda_{\xi p}(i-1)\bar{M} + B_{i-1}(I - M\bar{M})\bar{\Lambda}_p] \tag{A15}$$

For the first data interval it is reasonable to use Eq. (A1) to get $\Lambda_\xi(0)$ in order to initiate the sequential procedure described above.

Hence

$$\Lambda_\xi(0) = I + D_o\Lambda_{np}^T + \Lambda_{np}D_o^T + D_o\bar{\Lambda}_p D_o^T \tag{A16}$$

where

$$D_o = Q_1\begin{bmatrix} 0 \\ \bar{\Lambda}_p^{-1/2} - \Lambda_p^{-1/2} \\ 0 \end{bmatrix} \tag{A17}$$

$$\Lambda_{np} = E[n_a(o)p_o^T] = Q_1\begin{bmatrix} 0 \\ -\bar{\Lambda}_\rho^{-1/2} \\ 0 \end{bmatrix} \tag{A18}$$

References

[1] Curkendall, D. W. et al., "The Effects of Random Accelerations on Estimation Accuracy With Application to the Mariner 1969 Relativity Experiment," *Proceedings of the Conference on Experimental Tests of Gravitational Theories*, California Institute of Technology, Pasadena, Calif., Nov. 1970.

[2] Curkendall, D. W., "Problems in Estimation Theory with Application to Orbit Determination," Ph.D. thesis, 1971, Univ. of California at Los Angeles, Los Angeles, Calif.

[3] Ondrasik, V. J. and Rourke, K. H., "Application of New Radio Tracking Data Types to Critical Spacecraft Navigation Problems," *JPL Quarterly Technical Review*, Vol. 1, No. 4, pp. 116–131, Jet Propulsion Lab., Pasadena, Calif., Jan. 1972.

[4] Ingram, D. S. and Tapley, B. D., "Orbit Determination in the Presence of Unmodeled Accelerations," AAS Preprint No. 71-371, Astrodynamics Specialist Conference, Fort Lauderdale, Fla., Aug. 1971.

[5] Esposito, P. B. et al., "Classical Least Squares and Sequential Estimation Techniques as Applied to the Analysis of the Mariner VI and VIII Tracking Data," AAS Preprint No. 71-384, Astrodynamics Specialist Conference, Fort Lauderdale, Fla., Aug. 1971.

[6] Nishimura, T., "Modeling Errors in Kalman Filters," JPL Tech. Rept. 32-1319, June 1970, Jet Propulsion Lab., Pasadena, Calif.

[7] Griffin, R. E. and Sage, A. P., "Large and Small Scale Sensitivity Analysis of Optimum Estimation Algorithms," *IEEE Transactions on Automatic Control*, Vol. AC-13, No. 4, Aug. 1968, pp. 320–329.

[8] Hanson, R. J. and Lawson, C. L., "Extensions and Applications of the Householder Algorithm for Solving Linear Least Squares Problems," *Mathematics of Computation*, Vol. 23, Oct. 1969, pp. 787–812.

[9] Dyer, P. and McReynolds, S. R., "The Extension of Square-Root Filtering to Include Process Noise," *Journal of Optimization: Theory and Applications*, Vol. 3, June 1969, pp. 92–105.

[10] Kizner, W., "A Method of Describing Miss Distances for Lunar and Interplanetary Trajectories," External Publication No. 674, Aug. 1959, Jet Propulsion Lab., Pasadena, Calif.

APRIL 1974 J. SPACECRAFT VOL. 11, NO. 4

Coupled Librational Motions of a Gyrostat Satellite

FRANK C. LIU*
The University of Alabama, Huntsville, Ala.

This paper deals with coupled librational motions of a rigid gyrostat satellite in an elliptic orbit. The analysis is based on the assumptions that the orbital eccentricity is small and that the satellite is an aspherical rigid body with one or more rigidly attached gyro-rotors. The differential equations of the Euler angles are derived for the perturbed motion from gravitational equilibria in a circular orbit. Using the linearized system of equations as the basis, the equation of natural frequencies, and harmonic response are formulated. Periodic solutions of eccentricity forced motion are obtained by using a two-term Fourier series for the pitch motion and power series in eccentricity for the roll and yaw motions. A rigid gyrostat satellite having flexible appendages is also treated.

I. Introduction

PRECISE attitude control of an Earth-pointed orbiting satellite is very important to many space projects. The use of gyro-rotors as means of attitude control and stability analysis of the attitude motions of a satellite in a circular orbit have attracted numerous researchers in the last decade. The research works may be roughly divided into two categories according to the physical system of a satellite, namely, gyrostat satellites[1–8] and spinning satellite with flexible appendages.[9–11]

Effect of a rotor on the attitude stability of a gyrostat satellite was analyzed by Kane and Mingori[1] using Floquet theory. Breakwell and Pringle[2] applied the Hamilton-Jacobi theory to treat nonlinear resonance of a gyrostat satellite. The existence of four cases of gravitational equilibria for a rigid gyrostat satellite in a circular orbit was established by Roberson and Hooker[3] and the general solutions of these equilibria were obtained by Longman and Roberson.[4] The stability analysis of all possible equilibria were presented first by Rumyantsev[5] by using the principle of stationary points of a transformed potential energy and then by Longman[6] by Liapunov method. The infinitesimally stable and Liapunov stable regions for case 1 equilibria, as defined by Ref. 3, were presented in three dimensional plots of vehicle shape parameters by Crespo da Silva.[7] In Ref. 8, he also investigated nonlinear resonant attitude motions about case 1 equilibria both analytically and numerically.

Space vehicle control engineers are concerned with the existence of high frequency components of an orbiting vehicle in ground laboratory simulation tests. Great efforts, therefore, have been devoted to structural analysis of a flexible primary body connected with many elastic sub-bodies. This approach often requires lengthy computations and results in a large number of variables.

Stability analysis of a nonsymmetric gyrostat satellite for the cases 2 and 3 equilibria involves five parameters, instead of three for case 1. Determination of stable regions and nonlinear resonance by the method such as that used in Refs. 7 and 8 becomes a cumbersome task. The first part of this paper presents a study of a linearized attitude motions for cases 2 and 3 equilibria of a gyrostat satellite in a circular orbit. The second part concerns with solutions for the eccentricity forced attitude motions if the satellite orbit has a small eccentricity. The last part gives a simplified approach for dealing with dynamic coupling of a flexible appendage.

In this analysis we assume that: 1) a gyrostat satellite consists of an aspherical rigid primary body and one or more dynamically balanced rotors; 2) the axes of the rotors are rigidly attached to the primary body and the rotors have constant speeds relative to the primary body; and 3) for a satellite in an elliptical orbit, the magnitude of eccentricity is of the same order as the perturbed variables.

II. Analysis

A. Derivation of Equations of Motion

Let us consider that a gyrostat satellite consists of a rigid primary body and one or more dynamically balanced gyro-rotors

Received July 6, 1973; revision received October 29, 1973.
Index category: Spacecraft Attitude Dynamics and Control.
* Professor of Engineering. Member AIAA.